



University of Dundee

On solitary wave diffraction by multiple, in-line vertical cylinders

Neill, Douglas R.; Hayatdavoodi, Masoud; Ertekin, R. Cengiz

Published in:
Nonlinear Dynamics

DOI:
[10.1007/s11071-017-3923-1](https://doi.org/10.1007/s11071-017-3923-1)

Publication date:
2018

Document Version
Peer reviewed version

[Link to publication in Discovery Research Portal](#)

Citation for published version (APA):

Neill, D. R., Hayatdavoodi, M., & Ertekin, R. C. (2018). On solitary wave diffraction by multiple, in-line vertical cylinders. *Nonlinear Dynamics*, 91(2), 975-994. <https://doi.org/10.1007/s11071-017-3923-1>

General rights

Copyright and moral rights for the publications made accessible in Discovery Research Portal are retained by the authors and/or other copyright owners and it is a condition of accessing publications that users recognise and abide by the legal requirements associated with these rights.

- Users may download and print one copy of any publication from Discovery Research Portal for the purpose of private study or research.
- You may not further distribute the material or use it for any profit-making activity or commercial gain.
- You may freely distribute the URL identifying the publication in the public portal.

Take down policy

If you believe that this document breaches copyright please contact us providing details, and we will remove access to the work immediately and investigate your claim.

On Solitary Wave Diffraction by Multiple, In-line Vertical Cylinders

Douglas R. Neill

Masoud Hayatdavoodi

R. Cengiz Ertekin

Received: date / Accepted: date

Abstract The interaction of solitary waves with multiple, in-line vertical cylinders is investigated. The fixed cylinders are of constant circular cross-section and extend from the sea floor to the free surface. In general, there are N of them lined in a row parallel to the incoming wave direction. Both the nonlinear, generalized Boussinesq and the Green-Naghdi shallow-water wave equations are used. A boundary-fitted curvilinear coordinate system is employed to facilitate the use of the finite-difference method on curved boundaries. The governing equations and boundary conditions are transformed from the physical plane onto the computational plane. These equations are then solved in time on the computational plane that contains a uniform grid and by use of the successive over relaxation method and a second-order finite-difference method to determine the horizontal force and overturning moment on the cylinders. Resulting solitary wave forces from the nonlinear Green-Naghdi and the Boussinesq equations are presented, and the forces are compared with the experimental data when available.

D. R. Neill

National Optical Astronomy Observatory, 950 N Cherry Ave., Tucson, AZ 85719, USA

M. Hayatdavoodi

Civil Engineering Department, School of Science and Engineering, University of Dundee, Dundee DD1 4HN, UK

E-mail: mhayatdavoodi@dundee.ac.uk

R.C. Ertekin

Guest Professor, College of Shipbuilding Engineering, Harbin Engineering University, Harbin, China

Keywords Solitary wave · multiple inline vertical circular cylinders · wave force and moment · Boussinesq equations · Green-Naghdi equations

1 Introduction

Many marine structures are built on vertical cylinders; consequently, the determination of the forces which are a result of the wave-cylinder interaction is an important problem in ocean engineering. However, very few studies have considered nonlinear shallow-water wave equations to investigate solitary- and cnoidal-wave diffraction by vertical cylinders and calculated the forces and moments acting on it.

We consider here the interaction of solitary waves with fixed, multiple inline vertical cylinders of constant circular cross section. The cylinders extend from the seafloor to the free surface, and the still-water depth is held constant. Different shallow-water wave equations can produce different solitary waves, and may describe the flow field differently, and thereby can lead to different wave loads. Both the generalized Boussinesq (gB) (Wu (1981)) and the Green-Naghdi (GN) (Green and Naghdi (1977)) Level I equations are used to solve numerically the initial-boundary-value problem to obtain the horizontal forces and overturning moments on multiple cylinders in shallow water.

The linearized potential problem of wave diffraction by a single vertical cylinder was solved by MacCamy and Fuchs (1954) for an ideal fluid. The infinite depth solution of the same problem was obtained earlier by Havelock (1940). Scattering of waves for very long wave length (solitary wave) by a cylindrical object (island) was first solved by Omer and Hall (1949).

Only few investigations of nonlinear effects in the time domain exist compared with the linear ones. Isaacson (1983) studied the interaction of a solitary wave with an isolated cylinder by an approximate method by using the linear boundary conditions although the solitary wave problem has to be nonlinear. Isaacson and Cheung (1992) used a second-order time-domain method to investigate this problem. These studies showed good agreement between the numerical predictions and experimental data. Wang et al. (1992) used a generalized Boussinesq model to investigate the nonlinear effects of wave-cylinder interaction on hydrodynamic forces. Their investigation indicated that linear equations may produce wave forces that are 40% less than those predicted by nonlinear equations. Yang and Ertekin (1992) used the boundary-element method to solve the fully nonlinear diffraction problem to investigate the

34 diffraction of a solitary wave and Stokes waves by a vertical circular cylinder
35 in finite water depth; they solved Laplace's equation for an ideal fluid
36 subject to the exact boundary conditions to determine nonlinear wave diffraction
37 and loading. Neill and Ertekin (1997) studied the diffraction of solitary
38 waves by a vertical cylinder in shallow waters and presented some preliminary
39 results. More recently, Ghadimi et al. (2012) studied the diffraction of linear
40 waves by a floating, vertical circular cylinder and solved Laplace's equations
41 by use of the strip theory.

42 Most of the previous works have been extended to wave diffraction by
43 isolated cylinders, and the influence of neighboring cylinders is more limited.
44 McIver and Evans (1984) estimated the wave forces on a group of fixed, vertical
45 cylinders by solving Laplace's equation subject to linear boundary conditions,
46 and by use of an approximated method to account for the effect of neighboring
47 cylinders in the array. Similar approach was followed by Linton and Evans
48 (1990) to determine wave loads on an array of cylinders; they solved the linear
49 equations exactly, closely following a method suggested earlier by Spring and
50 Monkmeyer (1974). Other studies on wave diffraction by an array of vertical
51 cylinders include Malenica et al. (1999); Kagemoto et al. (2002); Han et al.
52 (2015); Kamath et al. (2015); Barlas (2012). Solitary wave interaction with a
53 group of vertical cylinders is studied by Mo and Liu (2009); Mo (2010) by use
54 of numerical models based on the Navier-Stokes and Euler's equations. Kudeih
55 et al. (2010) conducted laboratory experiments to study random wave loads
56 on an array of vertical cylinders in shallow water.

57 Our goal in this paper is to study the problem of diffraction of solitary
58 waves by multiple-inline vertical cylinders in shallow water, by use of the
59 Level I GN equations and the generalized Boussinesq equations, and discuss
60 the nonlinearity effect on the wave loads on the cylinders. Our objectives are
61 (i) to develop two models based on these well-known nonlinear, shallow-water
62 wave equations, (ii) to study the flow field and the wave impact on multiple
63 inline cylinders, including the effects of the neighbouring cylinders, and (iii)
64 to compare the results of these models with each other, and with the existing
65 data.

66 We first introduce the nonlinear shallow-water wave equations that we use
67 and formulate the initial-boundary-value problem and discuss the wavemaker
68 solutions of these equations. This is followed by the discussion on grid generation,
69 where we reformulate the problem in the computational plane after
70 transforming the problem from the physical plane. We then discuss the numer-

71 ical method used and finally present the results obtained for multiple in-line
72 cylinders. Both the predicted forces and moments on the vertical cylinders are
73 compared with the experimental data and predictions by others whenever they
74 are available, see e.g., Yates and Wang (1994). Finally, results are discussed
75 with an emphasis on how these two sets of shallow-water equations can predict
76 the flow field around multiple, in-line vertical cylinders.

77 **2 Theory**

78 A Cartesian coordinate system, whose origin is on the upwave or entrance
79 boundary where the numerical wave maker is located, is used. In this three-
80 dimensional system, the x -direction is along the line of symmetry, which also
81 is perpendicular to the incident wave crest-line. The y -direction is parallel to
82 the entrance boundary, and the z -direction is vertical, with positive z up, see
83 Fig 1. It is assumed that the vertical cylinders have constant, circular cross
84 section and the still-water depth, h , is held constant. The problem is symmetric
85 with respect to the line that passes through the in-line cylinders center and
86 is perpendicular to the wave crest-line. Since the problem is symmetric, only
87 one half of the physical region needs to be considered. The physical problem is
88 modeled as an initial-boundary-value problem. In Fig. 1, the upwave boundary
89 is where the numerical wavemaker is located and the downwave boundary is
90 the "open" boundary or absorbing boundary to prevent possible reflections
91 as much as possible. On the symmetry, far wall and the cylinder boundaries,
92 the normal component of the fluid velocities must vanish but we allow the
93 tangential component as the fluid is assumed to be inviscid in this work.

94 **2.1 Shallow-water wave equations**

95 The solitary wave scattering, horizontal forces and overturning moment on the
96 vertical, in-line cylinders are calculated in time by solving either the GN or
97 gB equations. In this section, the governing equations and assumptions made
98 in developing the theoretical models are discussed.

99 *2.1.1 The Green-Naghdi (GN) Equations*

100 The GN equations use the assumption that the fluid is incompressible and
101 homogeneous. In this study, the fluid is assumed inviscid, although this is not

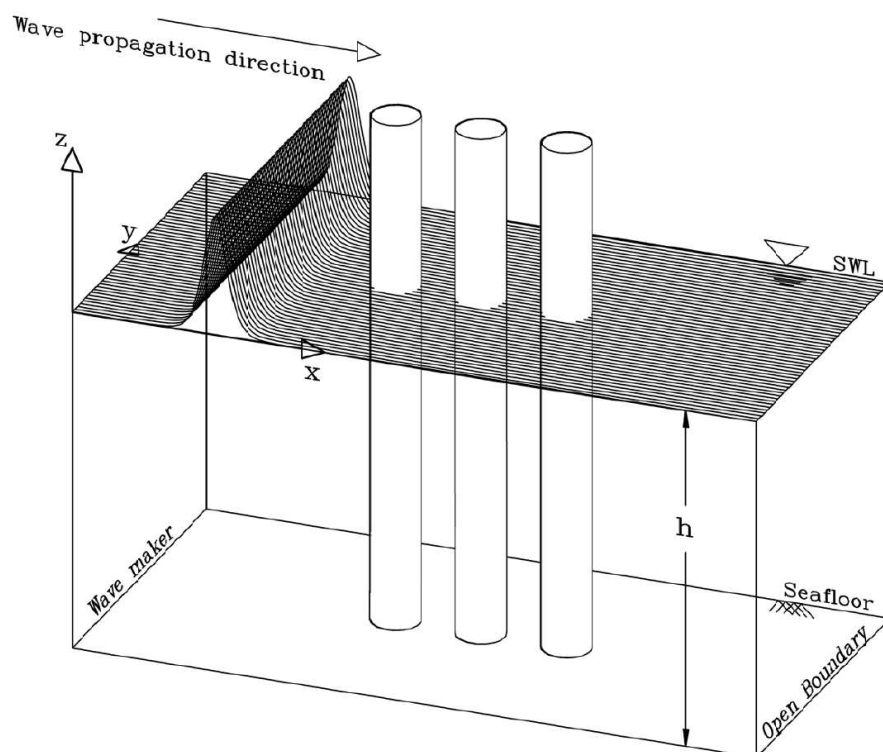


Fig. 1 Schematic of the numerical wave tank, showing different boundaries discussed in the text, and showing three in-line cylinders. Not to scale.

102 a requirement for the GN equations in general, see Green and Naghdi (1984).
 103 The derivation of the equations does not require the flow to be irrotational,
 104 therefore, the velocity potential does not exist. Investigations of these equa-
 105 tions were made by Green and Naghdi (1976a,b); Ertekin (1984); Ertekin et al.
 106 (1986); Ertekin (1988); Shields and Webster (1988); Demirbilek and Webster
 107 (1992); Ertekin et al. (2014), among others.

108 Unlike the Boussinesq-class equations, the GN equations do not follow
 109 from a perturbation expansion. The order of error, therefore, cannot be de-
 110 fined. The range of applicable wave lengths and heights must be determined by
 111 comparisons with experimental data. The kinematic and dynamic free-surface
 112 conditions are satisfied exactly. However, the conservation equations are satis-
 113 fied exactly in the depth averaged sense only. Ertekin (1984) obtained rather
 114 a classical form of the GN equations (see also Ertekin et al. (1986)). The GN
 115 equations can be specialized to our case by setting the pressure on the top

116 surface of the fluid sheet (\hat{p}) to atmospheric, and further assume that it is
 117 negligible, and by setting the water depth to constant ($\alpha = 0$) in the original
 118 equations given by Ertekin (1984):

$$\zeta_t + \nabla \cdot \{(h + \zeta)\mathbf{V}\} = 0, \quad (1)$$

$$\dot{u} + g\zeta_x = -\frac{1}{3}\{2\zeta_x\ddot{\zeta} + (h + \zeta)\ddot{\zeta}_x\}, \quad (2)$$

$$\dot{v} + g\zeta_y = -\frac{1}{3}\{2\zeta_y\ddot{\zeta} + (h + \zeta)\ddot{\zeta}_y\}, \quad (3)$$

119 where h is the constant water depth, g is the gravitational acceleration, ζ is
 120 the free surface elevation measured from the still-water level, and ∇ is the
 121 gradient vector operator, $\nabla = (\partial/\partial x)\mathbf{e}_1 + (\partial/\partial y)\mathbf{e}_2$, and $\mathbf{V} = u\mathbf{e}_1 + v\mathbf{e}_2$ is
 122 the particle velocity vector on the horizontal plane as these are assumed to
 123 not depend on the vertical z coordinate in the Level I GN equations. In higher
 124 level GN equations, however, they would depend on the z coordinate, see e.g.,
 125 Shields and Webster (1988); Zhao et al. (2014a, 2015). \mathbf{e}_1 and \mathbf{e}_2 are the unit
 126 base vectors in the x and y directions, respectively. It is understood that the
 127 subscripts denote differentiation with respect to them. The superposed dot
 128 denotes the material time derivative, i.e., for any physical quantity f , we have
 129 $\dot{f} = f_t + uf_x + vf_y$. A double superposed dot denotes the second material time
 130 derivative. Note that Eq. (1) is a statement of conservation of mass and Eqs.
 131 (2) and (3) are statements of conservation of linear momentum and director
 132 momentum (moment of momentum) combined, in the x and y directions,
 133 respectively.

134 The following dimensionless variables are used in this study by selecting
 135 (ρ, g, h) as a dimensionally independent set:

$$\bar{t} = \frac{t}{h} \sqrt{gh}, \quad \bar{F} = \frac{F}{\rho gh^2 R}, \quad \bar{M} = \frac{M}{\rho gh^3 R}, \quad \bar{P} = \frac{P}{\rho gh}, \quad (4)$$

136 where the bars represent the dimensionless quantities, and ρ is the mass den-
 137 sity, F is the horizontal force on the cylinder, M is the overturning moment
 138 with respect to the sea floor, P is the pressure, and R is the cylinder radius.
 139 Any quantity whose dimension is length is scaled by h and any quantity which
 140 has the dimension of velocity is scaled by \sqrt{gh} . The same nondimensionaliza-
 141 tion is used for the gB equations and the linear equations and the bars over the
 142 physical quantities will be dropped for convenience unless otherwise stated.

143 A close look at Eqs. (2) and (3) shows that they involve the second order
 144 time derivative of the surface elevation. By combining the definition of mate-

145 rial derivative with the continuity equation, Eq. (1), a new equation for the
 146 second derivative of ζ can be obtained. This procedure results in removing the
 147 difficulties associated with the presence of the time derivatives of the surface
 148 elevation on the right-hand sides of Eqs. (2) and (3). As discussed by Qian
 149 (1994), this is accomplished by first isolating ζ_t in Eq. (1) and then substi-
 150 tuting it into the first material derivative of ζ . As a result, the first material
 151 derivative of ζ no longer contains a partial derivative with respect to time, t ,
 152 i.e., $\dot{\zeta} = -\nabla \cdot [(h + \zeta)\mathbf{V}] + \mathbf{V} \cdot \nabla \zeta$. The local time derivative of the surface
 153 elevation, ζ , is again removed from its second material derivative to obtain
 154 $\ddot{\zeta} = (h + \zeta)[(u_x + v_y)^2 - (u_{tx} + v_{ty}) - u(u_{xx} + v_{xy}) - v(u_{xy} + v_{yy})]$. Substituting
 155 these into Eqs. (2) and (3) produces a set of component equations that do
 156 not contain the second derivatives with respect to time, and this is a very
 157 significant step to efficiently and accurately obtain the numerical solutions of
 158 these equations. The dimensionless form of the GN equations, Eqs. (1)-(3), af-
 159 ter eliminating the time derivatives of ζ from the right-side of the momentum
 160 equations can be obtained as

$$\zeta_t = -\zeta_x u - \zeta_y v - (\zeta + 1)(u_x + v_y), \quad (5)$$

161

$$\begin{aligned} u_t - (\zeta + 1)\zeta_x (u_{xt} + v_{yt}) - \frac{1}{3}(\zeta + 1)^2 (u_{xxt} + v_{xyt}) &= -\zeta_x - uu_x - vv_y \\ - (\zeta + 1)\zeta_x \left[(u_x + v_y)^2 - u(u_{xx} + v_{xy}) - v(u_{xy} + v_{yy}) \right] - \frac{1}{3}(\zeta + 1)^2 &\cdot \\ \cdot ((u_x + 2v_y)(u_{xx} + v_{xy}) - v_x(u_{xy} + v_{yy}) - u(u_{xxx} + v_{xxy}) - v(u_{xxy} + v_{xyy})) &, \end{aligned} \quad (6)$$

$$\begin{aligned} v_t - (\zeta + 1)\zeta_y (u_{xt} + v_{yt}) - \frac{1}{3}(\zeta + 1)^2 (u_{xyt} + v_{yyt}) &= -\zeta_y - uv_x - vv_y \\ - (\zeta + 1)\zeta_y \left[(u_x + v_y)^2 - u(u_{xx} + v_{xy}) - v(u_{xy} + v_{yy}) \right] - \frac{1}{3}(\zeta + 1)^2 &\cdot \\ \cdot [(2u_x + v_y)(u_{xy} + v_{yy}) - v_y(u_{xx} + v_{xy}) - u(u_{xxy} + v_{xyy}) - v(u_{xyy} + v_{yyy})] &. \end{aligned} \quad (7)$$

162 2.1.2 The generalized Boussinesq (gB) Equations

163 We use the generalized Boussinesq equations based in the form derived by Wu
 164 (1981) for constant water depth and for zero atmospheric pressure. We give
 165 here the dimensionless form of these equations after we use Eq. (4) and remove

166 the bars over the quantities:

$$\zeta_t + \nabla \cdot \{(1 + \zeta) \nabla \phi\} = 0, \quad (8)$$

167

$$\phi_t + \frac{1}{2} \|\nabla \phi\|^2 + \zeta = \frac{1}{3} \nabla \phi_t, \quad (9)$$

168 where ϕ is the layer-mean velocity potential. These equations assume an in-
 169 compressible and inviscid fluid. The use of the layer-mean velocity potential,
 170 also requires the assumption of irrotationality of the flow. The bottom no-flux
 171 condition as well as the kinematic and dynamic free-surface conditions are
 172 satisfied approximately in the derivation of the gB equations.

173 The first gB equation, Eq. (8), is simply the continuity equation and repre-
 174 sents the conservation of mass statement. The second equation, Eq. (9), follows
 175 from the momentum equation, and is obtained using perturbation methods.
 176 Therefore, the conservation of momentum is satisfied only approximately. The
 177 error is of order $(\alpha\epsilon^4, \alpha^2\epsilon^2)$ as shown by Wu (1981), where $\alpha = A/h$, $\epsilon = h/L$,
 178 where A is the wave amplitude and L is the wave length. The two param-
 179 eters, α and ϵ , represent the nonlinear and dispersive behaviors of waves,
 180 respectively. For the gB equations, both parameters are assumed to be small,
 181 $O(\alpha) = O(\mu^2) < 1$, where $\mu = kh = 2\pi\epsilon$. The gB equations are most applicable
 182 when the Ursell parameter, $U_r = \alpha/\mu^2$, is of $O(1)$.

183 The gB equations are not used here in the common form given by Eqs. (8)
 184 and (9) (as was done by Ertekin et al. (1990)) mainly for reasons of convenience
 185 in programming. The layer-mean velocity potential is instead eliminated from
 186 the equations by using the definition of the velocity potential. The layer-mean
 187 velocity potential is the average of the 3-D velocity potential over the depth
 188 of the fluid. This is in contrast to the 3-D velocity potential which represents
 189 the flow state at a specific point in time. The Eqs. (8) and (9) then are written
 190 in nondimensional component form as

$$\zeta_t + \nabla \cdot \{(1 + \zeta) \mathbf{V}\} = 0, \quad (10)$$

191

$$\dot{u} = u_t + uu_x + vu_y + \zeta_x = \frac{1}{3} (u_{xx} + u_{yy})_t = \frac{1}{3} \Delta u_t, \quad (11)$$

192

$$\dot{v} = v_t + uv_x + vv_y + \zeta_y = \frac{1}{3} (v_{xx} + v_{yy})_t = \frac{1}{3} \Delta v_t, \quad (12)$$

193 where Δ is the 2-D Laplacian on the horizontal plane. Clearly, this set of
 194 equations are simpler than the GN equations, (5)-(7), as there are less number
 195 of terms and derivatives involved.

2.2 Initial and Boundary Conditions

The initial conditions are chosen to correspond to a quiescent fluid, i.e., $\zeta(x, y, 0) = u(x, y, 0) = 0$. Therefore, the velocities and surface elevations are initially set to zero at which time the incident waves are located outside the computational domain on the upwave side. The boundary conditions along the line of symmetry, the surface of the cylinder, and the far wall, are the no-flux condition. This line of symmetry is along the wave propagation direction. The symmetry axis acts like a rigid surface, therefore, no flow is allowed through this surface. The normal velocity (v) therefore is equal to zero. The downwave boundary is an open boundary. The waves must be absorbed by this boundary without reflection. At the upwave boundary, the wavemaker solution, will be presented in subsequent sections for the solitary wave.

The sea-floor no-flux condition, as well as the kinematic and dynamic free-surface conditions, are accounted for directly in the derivations of the gB (approximately) and GN (exactly) equations, and therefore, they are not given here. See Green and Naghdi (1976a) and Wu (1981) for details on how the boundary conditions are embedded into the GN and gB equations, respectively.

Although we use a large computational domain for greater accuracy, it is necessary to use an absorption boundary on the downwave side. Previous works of Wu and Wu (1982) and Ertekin (1984) showed that the relatively simple Orlandi's condition with constant phase speed $c = \pm\sqrt{gh}$ prevents significant reflections from the open-boundary. We use this open-boundary condition here which reads

$$\Omega_t + c\Omega_x = 0, \quad (13)$$

where Ω may be $\zeta(x, t)$ or $u(x, t)$ at the downwave boundary.

It is noted that after the solitary wave has completely entered into the computational domain through the upwave boundary, the upwave boundary converts to the Orlandi condition, Eq. (13) (see e.g., Ertekin et al. (1986)) to absorb any reflected waves, similar to the downwave boundary.

We note that with regards to the implementation of the open boundary condition, Eq. (13), the use of the incident wave speed on the downwave open boundary instead of the linear wave speed provides superior wave absorption. Since this boundary needs to absorb supercritical solitary waves, the introduction of the incident wave speed in the Orlandi condition allows this radiation boundary to absorb the remainder of the incident wave after it had traversed

230 the entire domain. The upwave boundary where the wavemaker is located need
 231 to absorb any reflections due to the diffraction of solitary waves, and therefore,
 232 the linear long-wavelength limit, $c = \sqrt{gh}$, is used for the wave speed in the
 233 Orlanski condition on the upwave boundary. We monitored the wave eleva-
 234 tions at various numerical wave gauges and observed that the open-boundary
 235 conditions work well with minimum amount of reflections.

236 2.3 Wave-maker solutions

237 There are different types of solitary wave solutions. Some shallow-water equa-
 238 tions provide an analytic solitary-wave solution (as in the GN equations used
 239 here) and others need to be calculated numerically (as in the gB equations
 240 used here).

241 2.3.1 GN Solitary Wavemaker

242 An analytic solitary wave solution of the the GN Level I equations can be
 243 found in Green and Naghdi (1976a), and in Ertekin (1984), who has studied
 244 a number of constrained domain problems in shallow water involving solitons.
 245 The dimensional solitary-wave solution of the GN equations is given by¹

$$\zeta(x') = A \operatorname{sech}^2(\tau x'), \quad (14)$$

246 where

$$\tau = \sqrt{\frac{3A}{4h^2(A+h)}}. \quad (15)$$

247 and A is the amplitude of the solitary wave measured from the still-water level
 248 and is given by

$$A = \frac{c^2}{g} - h \quad \text{or} \quad \frac{c}{\sqrt{gh}} = \sqrt{1 + \frac{A}{h}}, \quad (16)$$

249 where c is the speed (critical or supercritical, or the depth Froude num-
 250 ber $Fr = U/\sqrt{gh} \geq 1$) of the wave, h is the constant water depth and
 251 $x' = x - x_0 - Ut$, where x_0 is the midpoint of the solitary wave at time
 252 $t = 0$. The horizontal velocity can be determined from the conservation of
 253 mass equation in the moving coordinates, $u = c\zeta/(1 + \zeta)$. Hayatdavoodi and

¹ This solution is the same as given by Rayleigh (1876).

254 Ertekin (2015c) presented a closed-form of the GN solitary wave horizontal
 255 and vertical velocities as

$$u(x', 0) = \sqrt{g(A+h)} \frac{A \operatorname{sech}^2(\tau x')}{h + A \operatorname{sech}^2(\tau x')}, \quad (17)$$

$$w(x', z, 0) = \frac{z+h}{h + A \operatorname{sech}^2(\tau x')} (2A \operatorname{sech}^2(\tau x') \tanh(\tau x')) \left(\sqrt{g(A+h)} - u \right). \quad (18)$$

256 Since the solitary wave in theory has an infinite length, it is not necessary
 257 to modulate it as long as it is located well to the left of the upwave boundary
 258 at time $t = 0$. Discussion on the steady, solitary-wave solution of high-level
 259 GN equations can be found in Zhao et al. (2014b).

260 2.3.2 gB Solitary Wavemaker

261 The solitary wave solution of the gB equations uses the same numerically
 262 determined wave solution used by Qian (1994); Roddier and Ertekin (1999)
 263 (see also Teng and Wu (1992)). This solution is found by eliminating the time
 264 derivatives from the gB equations by converting them to the moving or wave
 265 coordinates. The gB equations then can be combined into a single differential
 266 equation:

$$\zeta_x^2 = \frac{6}{Fr^2} (1+\zeta)^4 \ln(1+\zeta) + \left(2 + \frac{6}{Fr^2} \right) (1+\zeta)^4 - \left(3 + \frac{6}{Fr^2} \right) (1+\zeta^3) + (1+\zeta), \quad (19)$$

267 where $Fr = c/\sqrt{gh}$ is the depth Froude number and c is the dimensional wave
 268 celerity as before. The wave profile then is determined iteratively from Eq.
 269 (19). The amplitude, A , of the soliton is input into Eq. (19) as the initial value
 270 of ζ at the wave crest. We then use the 4th-order Runge-Kutta method to
 271 determine the slope for other values of x' to determine $\zeta(x')$ at the next step
 272 $x'_{i+1} = x'_i + \Delta x'$. This process is repeated until the wave profile is completed,
 273 also see e.g., Roddier (1994); Neill (1996) for more details.

2.4 Force and Moment Calculations

2.4.1 GN Equations

Ertekin (1984) provided closed-form relations for the integrated pressure (over the water depth) and the bottom pressure (on the seafloor). These relations are given by

$$P_I(x, y, t) = \frac{1}{6}(1 + \zeta)^2 (2\ddot{\zeta} + 3), \quad p(x, y, t) = \frac{1}{2}(1 + \zeta) (\ddot{\zeta} + 2), \quad (20)$$

respectively.

The total wave force on the cylinder is obtained by numerically integrating the pressure P_I around the circumference of the cylinder in the direction of the unit normal vector on the cylinder. The horizontal force component is then obtained by taking its x -component.

A difficulty exists in determining the resulting overturning moment for the GN equations. There is neither an expression for the moment nor an expression for the pressure as a function of depth that would allow the calculation of the moment. This difficulty is overcome here by assuming that the variation of the total pressure is linear with depth (equal to zero on the free surface and equal to the sea floor pressure on the bottom). This assumption is in close agreement with the pressure distribution predicted by the gB equations. This will be further discussed in the Results and Discussion Section. The error associated to the assumption of linear variation of pressure can be estimated, and indeed it is very small, as we will discuss later in this section.

The depth-varying pressure reads

$$P(x, y, z, t) = \frac{1}{2}(\zeta - z) (\ddot{\zeta} + 2). \quad (21)$$

Therefore, to determine the equation for the overturning moment with respect to the sea floor, Eq. (21) is multiplied by the moment arm, and then integrated over the depth:

$$M_I(x, y, t) = \int_{-1}^{\zeta} (1 + z) P(z) dz = \frac{1}{12}(1 + \zeta)^3 (\ddot{\zeta} + 2). \quad (22)$$

The moment acting on the cylinder can then be determined numerically by integrating the x -component of M_I around the circumference of the cylinder. See, e.g., Hayatdavoodi and Ertekin (2015b,a), for an approach to determine

301 the wave-induced loads on horizontal objects by use of the Level I GN equa-
 302 tions.

303 To determine the error of using Eq. (21) in approximating the pressure
 304 distribution in the z direction, we integrate $P(x, y, z, t)$ of Eq. (21) over the
 305 water depth:

$$P_{IL}(x, y, t) = \int_{-1}^{\zeta} P(x, y, z, t) dz = \frac{1}{4} (1 + \zeta)^2 (\ddot{\zeta} + 2). \quad (23)$$

306 The percent error, ϵ , made by the assumption of linearly-varying total pres-
 307 sure along the water column is then determined by comparing the integrated
 308 (linearly-varying) pressure, P_{IL} , with the integrated pressure of the GN equa-
 309 tions given by Eq. (20):

$$\epsilon = \left| \frac{P_I - P_{IL}}{P_I} \right| \times 100 = \left| \frac{\ddot{\zeta}}{4\zeta + 6} \right| \times 100. \quad (24)$$

310 Although Eq. (24) determines the error produced by the integrated pressure,
 311 it also is a reasonable estimate of the error produced by the moment equation
 312 (22). This error is determined for every node along the cylinder boundary and
 313 then an average is calculated. This average is then used as an approximate
 314 error value in the moment calculations as discussed later in Section 5.3.

315 2.4.2 gB Equations

316 Unlike the GN equations, the pressure as a function of depth is provided by the
 317 gB equations in terms of the layer-mean potential, see Wu (1981). However,
 318 we write the gB pressure equation in dimensionless velocity form:

$$P(z) = \zeta - z + \left(z + \frac{1}{2}z^2 \right) \nabla \cdot \mathbf{V}_t, \quad (25)$$

319 To facilitate the determination of the force, we integrate Eq. (25) over the
 320 water column and obtain

$$P_I = \frac{1}{2} (1 + \zeta)^2 + \frac{1}{6} (1 + \zeta) (\zeta^2 + 2(\zeta - 1)) \nabla \cdot \mathbf{V}. \quad (26)$$

321 Multiplying Eq. (25) by the moment arm and integrating over the depth
 322 gives the expression for the overturning moment (about the y axis) with respect

323 to the seafloor:

$$M_I = \frac{1}{6} (1 + \zeta)^3 + \frac{1}{8} (1 + \zeta)^2 \left((1 + \zeta)^2 - 2 \right) \nabla \cdot \mathbf{V}_t. \quad (27)$$

324 Finally, the integrated pressure and moment, P_I and M_I , are numerically
 325 integrated around the circumference of the cylinder in the direction of the unit
 326 normals on the cylinder to determine the horizontal force in the x direction
 327 and the overturning moment about the y axis, respectively.

328 **3 Grid Generation**

329 To facilitate the use of finite-difference methods to solve shallow water wave
 330 equations in the presence of irregular boundaries, numerical grid generation is
 331 used in this study. The use of numerical grid generation allows the inclusion
 332 of irregular boundaries conveniently by mapping the physical domain into a
 333 rectangular computational domain. The grid chosen for the computational
 334 domain is both regular and rectangular. This is not a requirement for the use
 335 of the grid-generation transformation system. It does, however, significantly
 336 reduce the complexity of the computations. The present study uses an elliptical
 337 generation technique in a connected 2-D region. Since the problem contains a
 338 symmetry axis, only one half of the region needs to be analyzed. Therefore, the
 339 grid system does not need to have re-entrant boundaries in either the physical
 340 or transformed plan.

341 The use of elliptical grid generation technique has been described exten-
 342 sively by, for example, Thompson et al. (1977). In this technique, a one-to-one
 343 mapping is developed between the physical plane and the computational plane
 344 by use of the Laplace equation. A uniform computational grid system with unit
 345 interval spacings is used in the solution of all the governing equations. This
 346 greatly simplifies the use of finite-difference methods. The minimization of the
 347 Euler integral ensures a one-to-one mapping. Details on the transformation
 348 of the governing equations as used in this work can be found in Qian (1988);
 349 Ertekin et al. (1990).

350 **4 Numerical Method**

351 We use the finite-difference method to solve the partial differential equations
 352 that govern the fluid motion. The difference equations are found through the

353 use of the second-order central difference formulas in space. To use the dif-
 354 ference equations along the boundaries, a fictitious point method is used. For
 355 example, along any boundary $x = x_1$, the equation for the first derivative
 356 would be

$$f'(x_1) = \frac{f(x_0) - f(x_2)}{2\Delta x} + O(\Delta x^2). \quad (28)$$

357 However, since x_0 is outside of the boundary, $f(x_0)$ is undefined. A fictitious
 358 value for $f(x_0)$ is found through a parabolic approximation: $f_0 = 3f_1 - 3f_2 + f_3$.
 359 By combining this equation with Eq.(28), a new equation is produced for the
 360 first derivative along the boundary:

$$f'(x_1) = \frac{-3f(x_1) + 4f(x_2) - f(x_3)}{2\Delta x} + O(\Delta x^2). \quad (29)$$

361 This method can be used to produce equations for all the derivatives along the
 362 boundaries, see Roddier (1994); Roddier and Ertekin (1999) for more details.

363 We use the time marching technique known as the modified Euler method,
 364 see e.g., Burden and Faires (1985). This two-step method has second-order
 365 accuracy. This method was also used successfully by Ertekin (1984); Ertekin
 366 et al. (1986); Roddier and Ertekin (1999); Hayatdavoodi and Ertekin (2015c),
 367 among others, in the solution of the GN and gB equations in 2-D.

368 The Successive Over-Relaxation (SOR) iterative method is used to solve
 369 the transformed forms of three sets of equations: GN Eqs. (5), (6), (7); and gB
 370 Eqs. (10), (11), (12). Two modifications are made to this method to improve
 371 the computational efficiency. Normally, the solution for u and v at the last
 372 time step is used as the initial guess for the next time step. In this analysis,
 373 however, the initial guess is extrapolated from the last two time steps using
 374 $u_{k+1}(i, j) - 2u_k(i, j) + u_{k-1}(i, j)$ and $v_{k+1}(i, j) - 2v_k(i, j) + v_{k-1}(i, j)$, where k is
 375 the time counter. Shown by Roddier and Ertekin (1999), this method reduces
 376 the number of SOR iterations by more than 40%. The second modification is
 377 to alternate the starting point and order of the iterations. Instead of always
 378 starting at $i = 1, j = 1$, the starting point is alternated between the four
 379 corners of the computational domain, $A(i = 1, j = 1)$, $D(i = 1, j = n)$, $E(i =$
 380 $m, j = 1)$ and $F(i = m, j = n)$. This technique also reduced the number of
 381 iterations.

382 The analysis carried out here requires filtering to remove numerical noise
 383 and ensure stability as pointed out by Ertekin et al. (1986). Much of this
 384 noise is the result of the central-difference scheme. When insufficient filtering
 385 is applied, the results become unstable. The third-order filtering by itself does

386 not provide sufficient stability. Our studies show that a combination of the
 387 five- (2nd order) and seven-point (3rd order) linear filtering schemes used here
 388 was developed by Shapiro (1975) and proved adequate to ensure stability.
 389 This includes the use of a third-order filtering in the direction normal to the
 390 prevailing wave crests, the ξ direction, and a second-order filtering parallel
 391 to the wave crests, the η direction. This does not modify the shape of the
 392 incoming waves. The filtering formulas that we use are given by

$$\begin{aligned} f_j &= \frac{1}{16} (-f_{j-2} + 4f_{j-1} + 10f_j + 4f_{j+1} - f_{j+2}), \\ f_i &= \frac{1}{64} (-f_{i-3} - 6f_{i-2} + 15f_{i-1} + 44f_i + 15f_{i+1} - 6f_{i+2} + f_{i+3}), \end{aligned} \quad (30)$$

393 where f is a generic variable that can represent ζ , u or v .

394 5 Error Monitoring

395 5.1 Conservation of Mass

396 To monitor the accuracy of the numerical solutions, the change in the mass
 397 due to numerical errors is determined following the approach used by Qian
 398 (1994); Roddier (1994). Conservation of mass is satisfied exactly for both the
 399 Green-Naghdi and the Boussinesq equations. Except for mass passing through
 400 the upstream or downstream boundaries, any change in mass is due to nu-
 401 merical errors. The Green-Naghdi equations exactly satisfy the conservation
 402 of momentum in the depth averaged sense, while the Boussinesq equations
 403 satisfy the momentum conservation approximately. Therefore, to monitor the
 404 numerical errors, the change in mass is chosen (preferred) here over the change
 405 in momentum or mechanical energy.

406 The total excess mass inside the physical domain (M), at a specific time,
 407 is determined by numerically integrating over the water column and over the
 408 surface area of the physical domain:

$$M = \int_A (1 + \zeta) dA. \quad (31)$$

409 The mass flow through the open boundaries is determined by integrating
 410 over these boundaries:

$$dm_{US} = \int_{US} (1 + \zeta) (\mathbf{v} \cdot \mathbf{n}) ds, \quad (32)$$

$$dm_{DS} = \int_{DS} (1 + \zeta) (\mathbf{v} \cdot \mathbf{n}) ds, \quad (33)$$

411 where, dm_{US} is the mass flow through the upstream boundary, and dm_{DS} is
 412 the mass flow through the downstream boundary. These boundaries are normal
 413 to the y-axis, therefore, the dot product of the velocity vector (\mathbf{v}) and the unit
 414 normal (\mathbf{n}) is simply the horizontal velocity in the x-direction (u). Therefore,
 415 Eqs. (32) and (33) are simplified to

$$dm_{US} = \int_{US} (1 + \zeta) u ds, \quad (34)$$

$$dm_{DS} = \int_{DS} (1 + \zeta) u ds. \quad (35)$$

416 These equations must also be integrated over time to determine the total
 417 loss or gain of mass across these boundaries.

$$dm_{US} = \int_t \int_{US} (1 + \zeta) (\mathbf{v} \cdot \mathbf{n}) ds dt', \quad (36)$$

$$dm_{DS} = \int_t \int_{DS} (1 + \zeta) (\mathbf{v} \cdot \mathbf{n}) ds dt', \quad (37)$$

418 where both the temporal and spacial integrations are performed numerically
 419 using Simpsons rule.

420 The total change in mass (dM_e) which is a result of numerical errors is
 421 found through the following relationship:

$$dM_e = M - M_0 - dM_{US} + dM_{DS}, \quad (38)$$

422 where M_0 is the initial total mass which is equal to ρV_D , where V_D is the
 423 volume of the quiescent body of fluid. The percent change in mass due to
 424 numerical errors can then be calculated through

$$M_E = \frac{dM_e}{M_0} * 100(\%). \quad (39)$$

425 The percent change in mass, as a function of time, is determined for each
 426 case. Some sample values for M_E for both the Green-Naghdi and the Boussi-

427 nesq solitary waves are given in Neill (1996). The maximum values of -0.20%
428 for the solitary wave are found to be the typical mass excess for the cases
429 studied here. In general, the solitary waves produce negative changes in mass.
430 The Green-Naghdi equations and the Boussinesq equations produced similar
431 mass change results.

432 5.2 Stability Conditions

433 It was shown by Ertekin (1984) through a Von Neumann stability analysis of
434 the linearized Green-Naghdi equations that Δt must be less than Δx for sta-
435 bility. This is equivalent to satisfying the Courant condition, which is accom-
436 plished by setting $\Delta t < \Delta x$ or Δy . Since the Boussinesq and Green-Naghdi
437 equations both linearize to the same equations, see Ertekin (1984), this sta-
438 bility analysis applies equally well to the Boussinesq equations. The nominal
439 values of Δt , Δx and Δy used are 0.20 , $0.25h$ and $0.33h$, respectively. Conse-
440 quently, this criteria is not violated in the grid systems that are used in this
441 study.

442 5.3 Green-Naghdi Moment Error

443 As discussed in Section 2.4, to determine the moment resulting from the Green-
444 Naghdi equations, a linear pressure distribution over the water depth is as-
445 sumed. The error caused by this assumption is determined through Eq. (24).
446 This error is determined for each cylinder and in every case analyzed. Ex-
447 amples of these errors are given for the Green-Naghdi solitary, and cnoidal,
448 waves in Neill (1996). It is shown that the moment error for the solitary wave
449 cases is less than 1.8% . This is primarily caused by the very large amplitude of
450 the solitary wave case considered ($A = 0.5h$). Given the simplifying assump-
451 tion made about the pressure distribution over the z direction, the error is
452 reasonably small.

453 6 Numerical Setup

454 The principle configuration for solitary waves in this study is a $4.0h$ diame-
455 ter cylinder and a $0.5h$ wave amplitude, unless otherwise is mentioned. This

456 configuration is used in many solitary wave cases and is chosen primarily to fa-
457 cilitate the comparison with other studies. Moreover, the $0.5h$ wave amplitude
458 is at the practical limit of use for the gB equations. According to Mei (1989),
459 these equations are applicable for $O(A) < 1$. This limit is a result of the as-
460 sumptions that led to the derivation of these equations. Although the GN
461 equations do not have an explicit limit, they must, nevertheless, have similar
462 implicit limitations. Any such limitations of the GN equations must be judged
463 by comparison with experiments.

464 The $4.0h$ cylinder diameter is also a convenient and reasonable size. This
465 size is large enough to produce significant diffraction, and is easily modeled
466 numerically. Smaller cylinders would require finer grids for the same accuracy
467 and viscous forces may become important. A larger diameter cylinder would
468 require a larger domain. Clearly, the latter two factors would increase the
469 computational time significantly.

470 The domain used includes a $20h$ distance from the upwave boundary to
471 the first cylinder surface, a $20h$ distance from the last cylinder surface to the
472 downwave boundary and a $20h$ distance from the far wall to the symmetry
473 axis. It will be shown later that this domain is large enough to avoid problems
474 of wave interactions at the boundaries that affect the resulting forces and
475 moments on the cylinders.

476 The nominal (dimensionless) grid sizes used in this domain are $\Delta x = 0.25$
477 and $\Delta y = 0.33$. These sizes are small enough to adequately model the surface
478 displacements and large enough to not require excessive CPU (central process-
479 ing unit) time. To insure stability, the time step must be smaller than the grid
480 size as discussed before. Therefore, the time step is chosen as $\Delta t = 0.2$.

481 7 Results and Discussion

482 Results of the GN and the gB equations for solitary wave interaction with ver-
483 tical cylinders are presented and discussed in this section. We will first start
484 by solitary wave interaction with a single cylinder and compare the results of
485 the theoretical models with the existing laboratory measurements and other
486 theories. This is then followed by results and discussion on solitary wave in-
487 teraction with two and three in-line vertical cylinders. We note that in this
488 study, and for the two and three cylinder configurations, all cylinders have the
489 same diameter.

490 7.1 Comparisons: Solitary Wave Interaction with a Single Cylinder

491 A comparison of time series of solitary wave force on a vertical cylinder, cal-
492 culated by the GN and the gB equations versus the laboratory experiments of
493 Yates and Wang (1994) is shown in Fig.2. In this case, the circular cylinder
494 diameter is $D = 3.18h$, and the wave amplitude is $A = 0.44h$. The wave force
495 and time are given in dimensionless form following Eq. (4).

496 In this comparison, both the GN and the Boussinesq models have slightly
497 overestimated the maximum and minimum values of the wave force, although
498 the GN equations are in closer agreement with the laboratory experiments.
499 Such discrepancy between the results of the GN and the Boussinesq models
500 with the laboratory measurements of Yates and Wang (1994) was previously
501 reported by Neill and Ertekin (1997), and was also observed by Yates and
502 Wang (1994) who compared results of their Boussinesq model with their own
503 laboratory measurements.

504 The laboratory experiments are conducted in a very small scale, and in
505 water depth of $h = 4cm$. The viscous effect, neglected in the inviscid the-
506 oretical models discussed here, may be noticeable at such small scales. Such
507 effects play a significant role on the slight differences between results. More-
508 over, the theoretical models are executed for the nominal wave amplitude of
509 $A = 0.44h$ corresponding to $A = 1.76cm$. Any small difference between the
510 wave amplitudes of the laboratory measurements and the theoretical models
511 would result in some differences in the wave forces. In the absence of any pre-
512 sentation of the undisturbed solitary waves in Yates and Wang (1994), this is
513 possibly another reason of the discrepancy, particularly noting that the travel-
514 ing speed of the wave in the laboratory is smaller than the two theories; see
515 the differences of the time of the force troughs in Fig.2. Recall from Eq. (16)
516 that solitary wave speed increases with larger wave amplitudes.

517 A comparison of the time series of the solitary wave force on a vertical
518 cylinder calculated by the GN and the gB models, with existing theoretical
519 solutions is shown in Fig. 3. In this case, the cylinder diameter is $D = 4.0h$
520 and the wave amplitude is $A = 0.5h$. In this comparison, the results of the
521 GN and the Boussinesq models are in good agreement with other theoretical
522 solutions, and fall between the BEM solution of Yang and Ertekin (1992) and
523 the gB model of Wang et al. (1992). The peak of the solitary wave force of
524 the GN model is in very close agreement with the BEM results, and is slightly
525 smaller than the Boussinesq results.

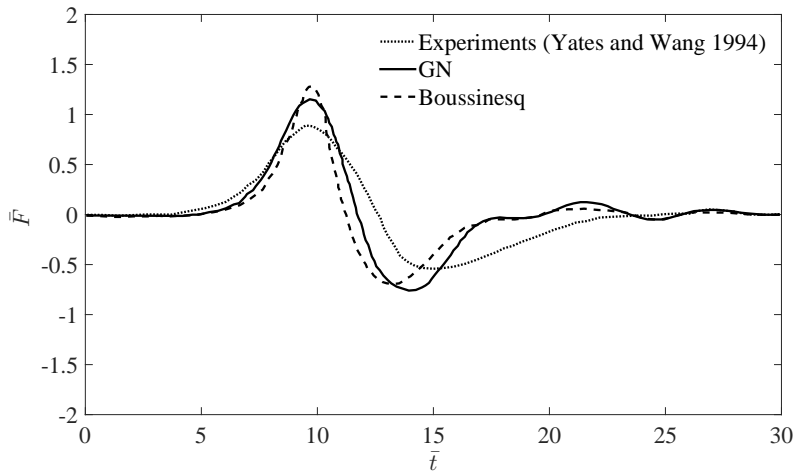


Fig. 2 Comparison of time series of solitary wave force on a single, vertical cylinder calculated by the GN and gB equations versus the laboratory experiments of Yates and Wang (1994). $A = 0.44h$ and $D = 3.18h$.

526 The analytical solution of Isaacson (1978) of wave force on the vertical
 527 cylinder has underestimated the force amplitude when compared to other so-
 528 lutions. In contrast, the Boussinesq model results of Wang et al. (1992) over
 529 estimates the force amplitude when compared to other results. Such overesti-
 530 mation appears to be due to the error associated to the mesh and the numerical
 531 solution of the equations. As discussed by Neill (1996), the wave run-up on the
 532 cylinder, and consequently the peak of the solitary wave forces, would increase
 533 if grid repulsion is not used, as in the Boussinesq model of Wang et al. (1992).
 534 The use of the grid repulsion improves the grid line orthogonality along the
 535 curved boundaries. The larger wave run-up in the Wang et al. (1992) model,
 536 also causes a larger wave reflection, resulting in smaller force trough when
 537 compared with the Boussinesq model discussed here, see Fig. 3.

538 Further results and discussion of the GN and the gB models on solitary
 539 wave interaction with a single cylinder can be found in Neill and Ertekin
 540 (1997).

541 7.2 Solitary Wave Interaction with Two Cylinders

542 The two cylinder solitary wave case also uses the same $4.0h$ diameter cylinder
 543 and $0.5h$ wave amplitude used before. This allows direct comparison with

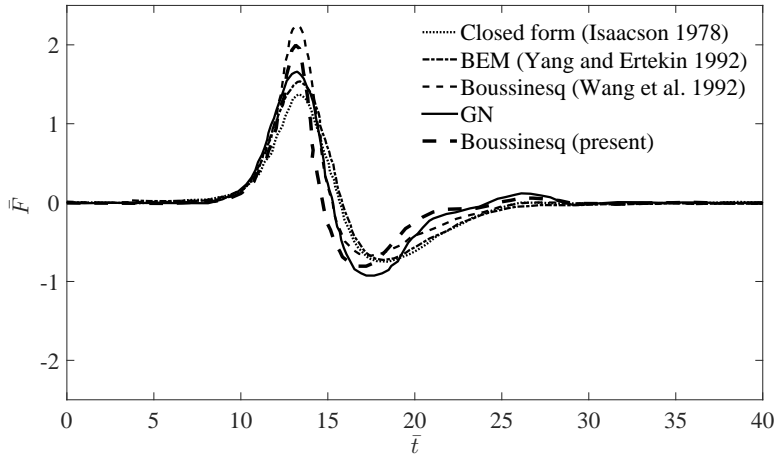


Fig. 3 Comparison of time series of solitary wave force on a single, vertical cylinder calculated by the GN and gB equations and existing theoretical solutions. $A = 0.5h$ and $D = 4.0h$.

544 Wang and Jiang (1994) who used the gB equations to study this configuration.
 545 Various spacings are used between the cylinders. In this section, the spacings
 546 used are $0.50D$, $0.75D$, $1.00D$, $2.00D$ and $3.00D$, where D , the diameter of
 547 the cylinder, is the same for both cylinders. The spacing between the two
 548 cylinders is measured as the closest distance between the cylinders. This is the
 549 same definition for spacing used by Wang and Jiang (1994). These spacings
 550 correspond to distances from the wave maker to the second cylinder center of
 551 $28h$, $29h$, $30h$, $34h$ and $38h$, respectively. Wang and Jiang (1994) also used the
 552 spacings of $0.0D$ and $0.25D$. For the $S = 0.0D$ spacing, the cylinder surfaces
 553 are in direct contact with each other.

554 Sample snapshots of the solitary wave surface elevations, calculated by
 555 the gB and the GN equations, are shown in Figs. 4 and 5, respectively. The
 556 resultant forces and moments in our study are shown in Figs. 6 and 7 for the
 557 gB equations and in Figs. 8 and 9. for the GN equations. Note that, the single
 558 cylinder results are also shown in these figures.

559 In general, the GN equations predict less shielding than the gB equations.
 560 Shielding is the reduction in force and moment on the downwave cylinder
 561 caused by the interaction of the waves on the upwave cylinder. The gB equa-
 562 tions predict a greater run-up on the first cylinder. This greater run-up causes
 563 more significant wave reflection and therefore there is a greater reduction in

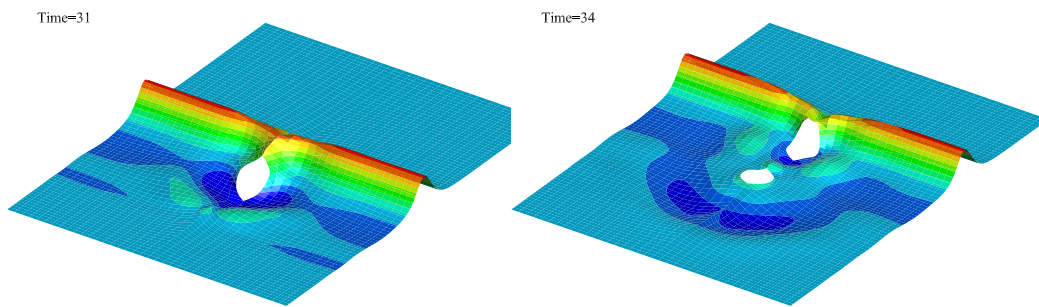


Fig. 4 3-D snapshots of solitary wave surface elevation around two cylinders, calculated by the gB equations, $S = 1.0D$, $D = 4.0h$ and $H = 0.5h$.

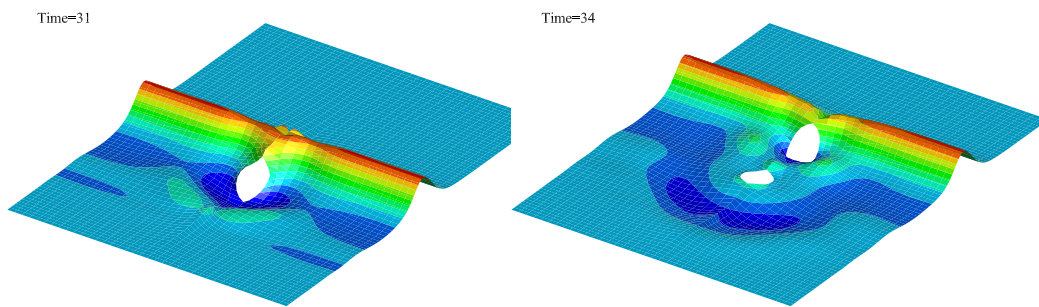


Fig. 5 3-D snapshots of solitary wave surface elevation around two cylinders, calculated by the GN equations, $S = 1.0D$, $D = 4.0h$ and $H = 0.5h$.

564 the wave amplitude downwave of the cylinder, and hence a greater reduction
 565 in the resulting force on the downwave cylinder.

566 The shielding described by Wang and Jiang (1994) is similar to the shield-
 567 ing found in this study. After the wave impacts the first cylinder, a 3-dimensional
 568 back-scattered wave emerges in front of the first cylinder. The primary wave
 569 deforms behind the first cylinder with a reduced wave amplitude. Therefore,
 570 the wave runup, force and moment are less for the second cylinder than the

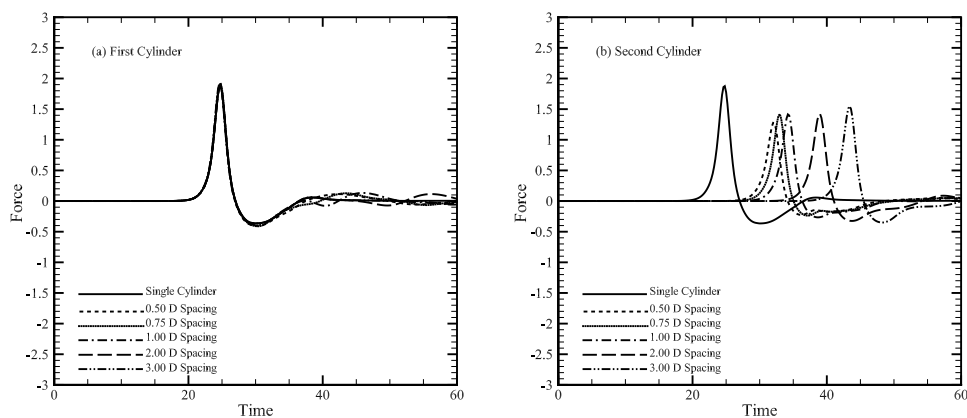


Fig. 6 Solitary wave forces on the (a) first and (b) second cylinder, for the two cylinder case, calculated by the gB equations, $H = 0.5h$, $D = 4.0h$.

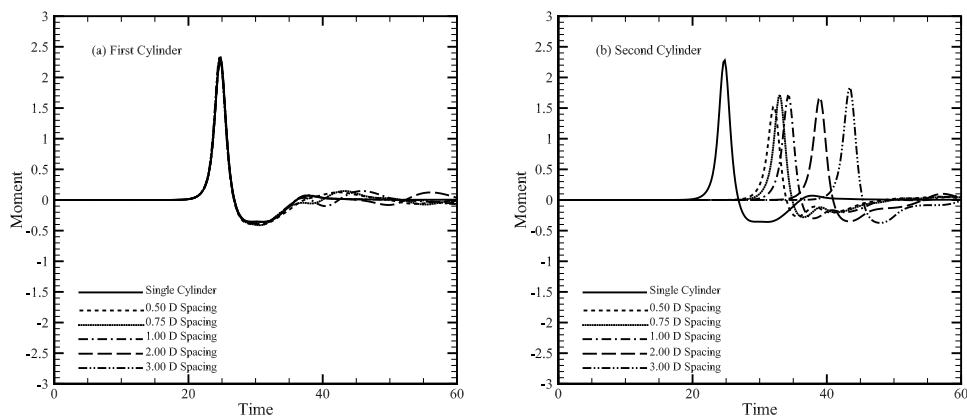


Fig. 7 Solitary wave moment on the (a) first and (b) second cylinder, for the two cylinder case, calculated by the gB equations, $H = 0.5h$, $D = 4.0h$.

571 first. The gB solution in this study consistently produces similar result to that
 572 of Wang and Jiang (1994), see Figs. 6 and 7. The small differences may be
 573 due to the lack of boundary orthogonality control in Wang and Jiang (1994)
 574 which causes the peak force value to be over-predicted. In both this study and
 575 Wang and Jiang (1994), the maximum force on the first cylinder is unaffected
 576 by the presence of the second cylinder. The maximum force on the second
 577 cylinder ($F_{max} = 1.60$), calculated by the gB equations in this study, is 21.6%

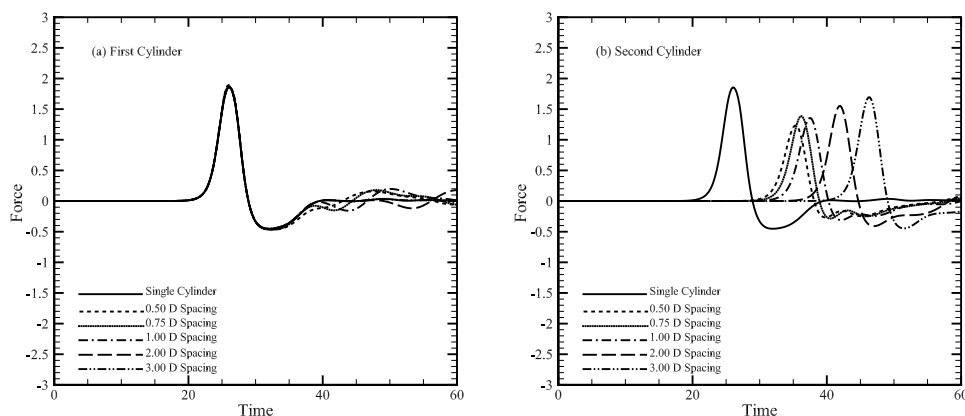


Fig. 8 Solitary wave forces on the (a)first and (b)second cylinder, for the two cylinder case, calculated by the GN equations, $H = 0.5h$, $D = 4.0h$.

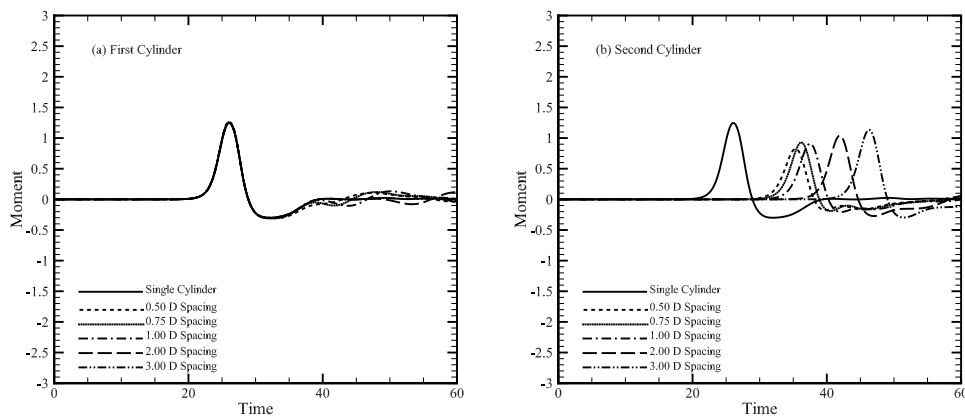


Fig. 9 Solitary wave moment on the (a)first and (b)second cylinder, for the two cylinder case, calculated by the GN equations, $H = 0.5h$, $D = 4.0h$.

578 smaller than that of the single cylinder case because of the presence of the
 579 first cylinder; the second cylinder is effectively shielded by the first cylinder.

580 In general, smaller distances between the cylinders leads to greater shield-
 581 ing and more force and moment reduction on the second cylinder as expected.
 582 A notable exception to this rule is the spacings of $0.0D$ and $0.25D$ used in
 583 Wang and Jiang (1994). For these spacings, there is a noticeable increase in
 584 both the maximum wave force on the second cylinder and the maximum neg-

585 active wave force on the first cylinder. This effect is also seen to a much smaller
 586 extent in the $0.5D$ spacing as shown in Figs. 6-8. The $0.0D$ and $0.25D$ spac-
 587 ings are not included in this work. It is concluded that sufficient boundary
 588 orthogonality control could not be produced for these small spacings to pro-
 589 duce more accurate results. It is unclear how much the forces of the $0.0D$ and
 590 $0.25D$ spacings causes calculated in Wang and Jiang (1994) were affected by
 591 any numerical error. The overturning moment on the cylinders show similar
 592 behaviour to the wave-induced horizontal force.

593 The GN solution shows much less reduction in the maximum force ($F_{max} =$
 594 1.48 , 11.4% reduction) for the second cylinder, see Figs. 8 and 9. In general, the
 595 shielding does become more pronounced, and the resulting force and moment
 596 on the second cylinder are reduced as the cylinder spacing is reduced. It should
 597 be noted that, although the force and moment reduction on the second cylinder
 598 is less for the GN solution, the actual force and moment on the second cylinder
 599 is still less than the equivalent force for the gB case. This is the result of the
 600 greater force and moment in the gB case, for the single cylinder.

601 7.3 Solitary Wave Interaction with Three Cylinders

602 For this case, a third cylinder with identical dimensions is added to the row.
 603 The $0.5h$ wave amplitude and $4.0h$ cylinder diameter are used again. The
 604 spacing between the second and third cylinders is equal to the spacing between
 605 the first and second cylinders. These spacings, $0.50D$, $0.75D$, $1.00D$, $2.00D$
 606 and $3.00D$ correspond to distances from the wave maker to the third cylinder
 607 center of $34h$, $36h$, $38h$, $46h$ and $54h$, respectively.

608 Samples of the solitary wave surface elevations for the three cylinder case,
 609 calculated by the gB and the GN equations, are shown in Figs. 10 and 11,
 610 respectively. The resulting forces and moments from the gB equations are
 611 shown in Figs. 12, 13 and 14. The resulting forces and moments from the GN
 612 equations are shown in Figs. 15, 16 and 17.

613 For both the gB and the GN equations, the forces and moment on the first
 614 and second cylinders of the three-cylinder case, see Figs. 12-17, are almost
 615 identical to those of the two-cylinder case, see Figs. 6-9. For both the gB and
 616 the GN equations, the force on the third cylinder is further reduced, see Figs
 617 12, 14, 16 and 17. As in the two-cylinder case, the maximum force reduction
 618 on the third cylinder is greater for the gB equations ($F_{max} = 1.42$, 30.4%
 619 reduction) than for the GN equations ($F_{max} = 1.40$, 16.2% reduction). The

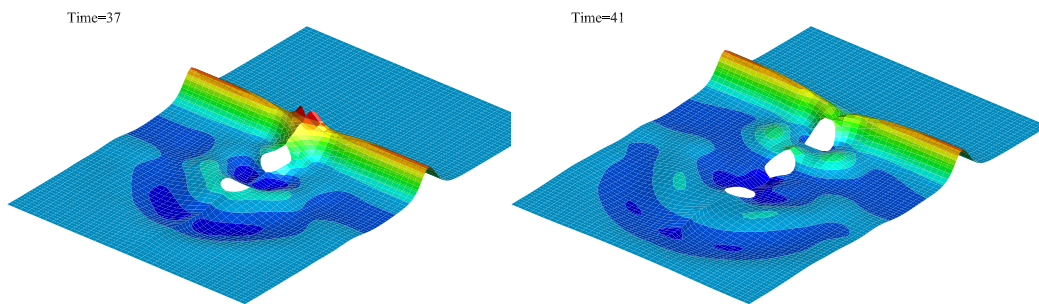


Fig. 10 3-D snapshots of solitary wave surface elevation around three cylinders, calculated by the gB equations, $S = 1.0D$, $D = 4.0h$ and $H = 0.5h$.

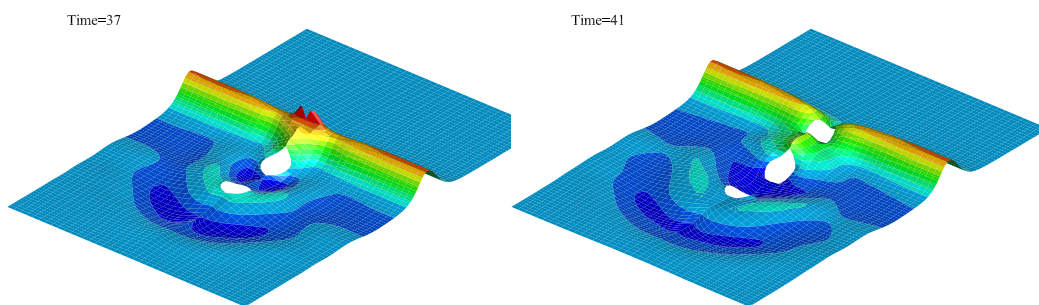


Fig. 11 3-D snapshots of solitary wave surface elevation around three cylinders, calculated by the GN equations, $S = 1.0D$, $D = 4.0h$ and $H = 0.5h$.

620 force and moment on the third cylinder, calculated by the gB equations, are
 621 similar in value to those of the GN equations. This is the result of the greater
 622 single-cylinder force and moment, and the greater force and moment reduction
 623 for the gB equations.

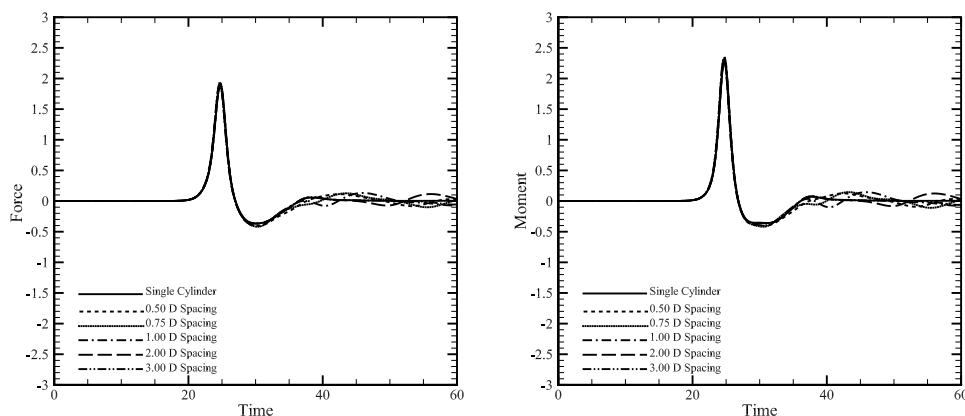


Fig. 12 Solitary wave forces and moments on the first cylinder of the three cylinder case, calculate by the gB equations, $H = 0.5h$, $D = 4.0h$.

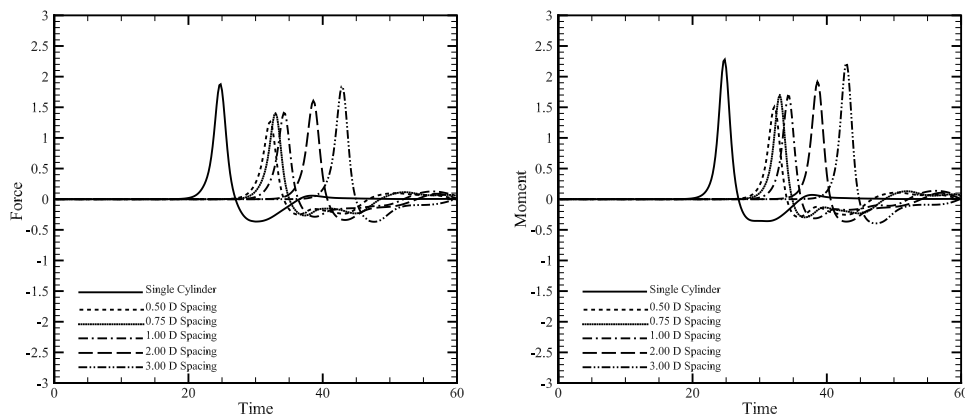


Fig. 13 Solitary wave forces and moments on the second cylinder of the three cylinder case, calculate by the gB equations, $H = 0.5h$, $D = 4.0h$.

624 7.4 Further Discussion on Solitary Wave Forces

625 The maximum forces resulting from solitary waves for the one, two and the
 626 three cylinder cases are shown in Figs. 18, 19 and 20. The single cylinder
 627 case corresponds to $(S/D) \rightarrow \infty$. The maximum force is the maximum absolute
 628 value of the horizontal force acting on the individual cylinders. The gB equa-
 629 tions, both in this study and in the earlier study of Wang and Jiang (1994),

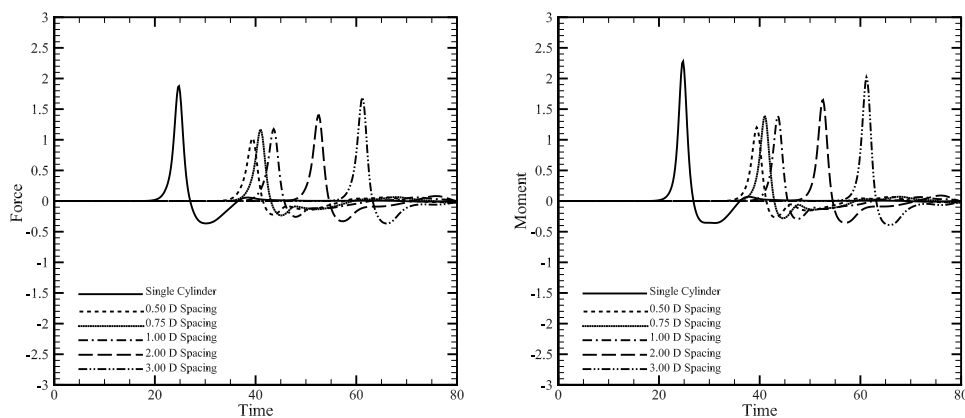


Fig. 14 Solitary wave forces and moments on the third cylinder of the three cylinder case, calculate by the gB equations, $H = 0.5h$, $D = 4.0h$.

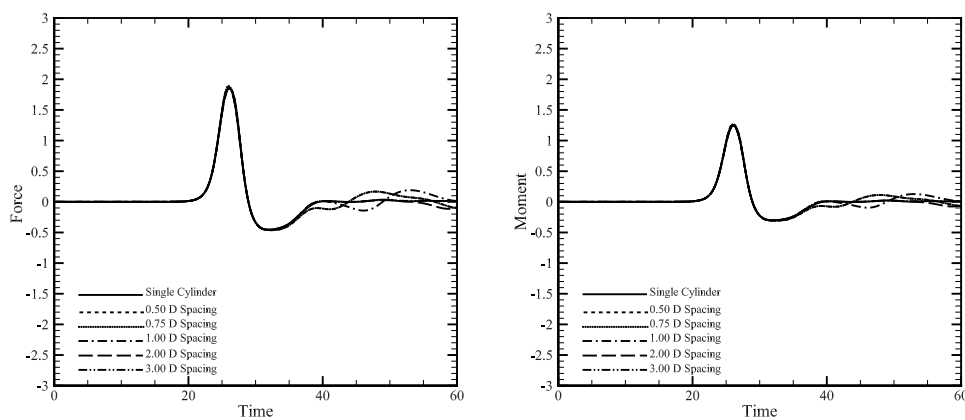


Fig. 15 Solitary wave forces and moments on the first cylinder of the three cylinder case, calculate by the GN equations, $H = 0.5h$, $D = 4.0h$.

630 showed that the upwave cylinders effectively shielded the downwave cylinders;
 631 see Figs. 19 and 20. The shielding effect is also predicted by the GN equa-
 632 tions, however, in smaller magnitude. Since the GN equations are in closer
 633 agreement with the experimental data, it is anticipated that the gB equations
 634 over-predict the amount of shielding. The closer the cylinders are together,
 635 the greater the shielding and the greater the reductions are. The third cylin-

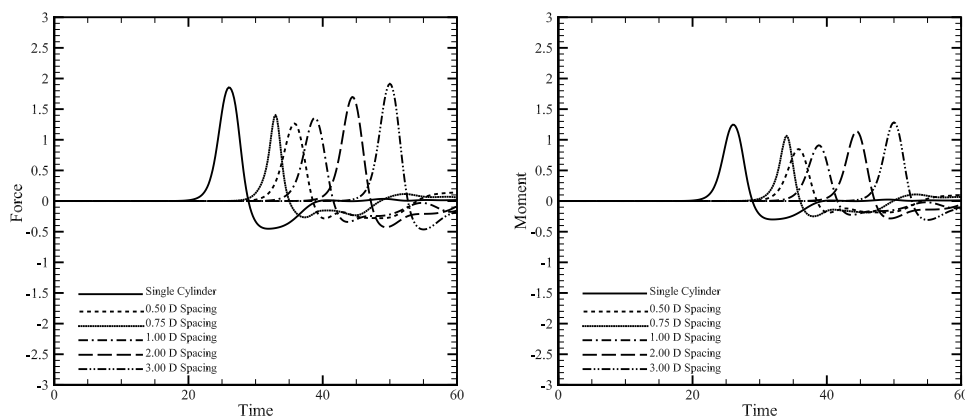


Fig. 16 Solitary wave forces and moments on the second cylinder of the three cylinder case, calculate by the GN equations, $H = 0.5h$, $D = 4.0h$.

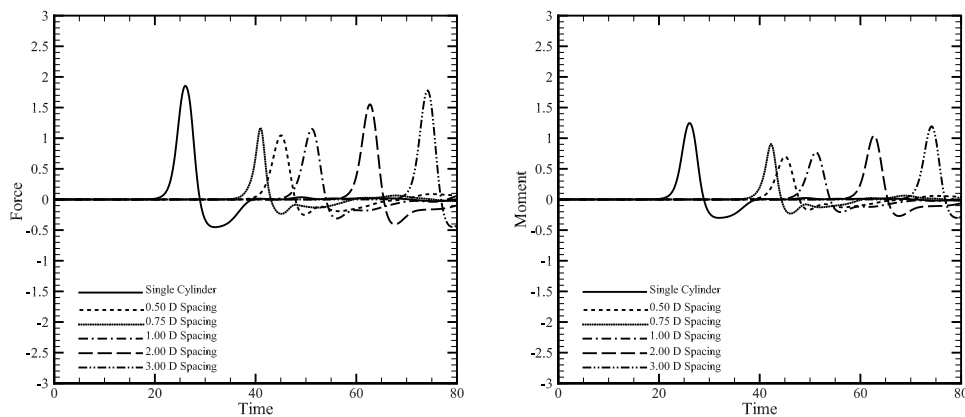


Fig. 17 Solitary wave forces and moments on the third cylinder of the three cylinder case, calculate by the GN equations, $H = 0.5h$, $D = 4.0h$.

636 der receives more shielding than the second cylinder. The downwave cylinders
637 have negligible effect on the upwave cylinders.

638 8 Concluding Remarks

639 The problem of interaction of solitary waves with multiple in-line fixed, verti-
640 cal, circular cylinders in shallow water is studied by use of the Green-Naghdi

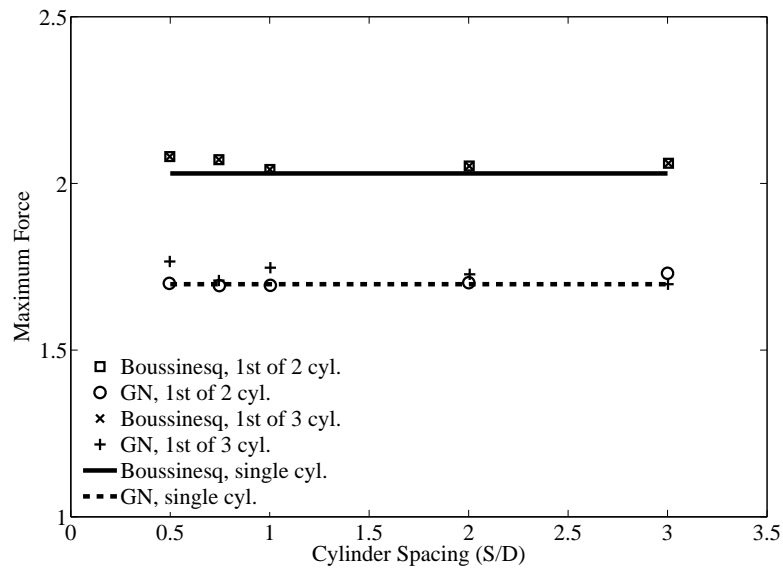


Fig. 18 Solitary wave maximum forces on the first cylinder, for one, two and three cylinders cases, versus cylinder spacing, $H = 0.5h$ and $D = 4.0h$

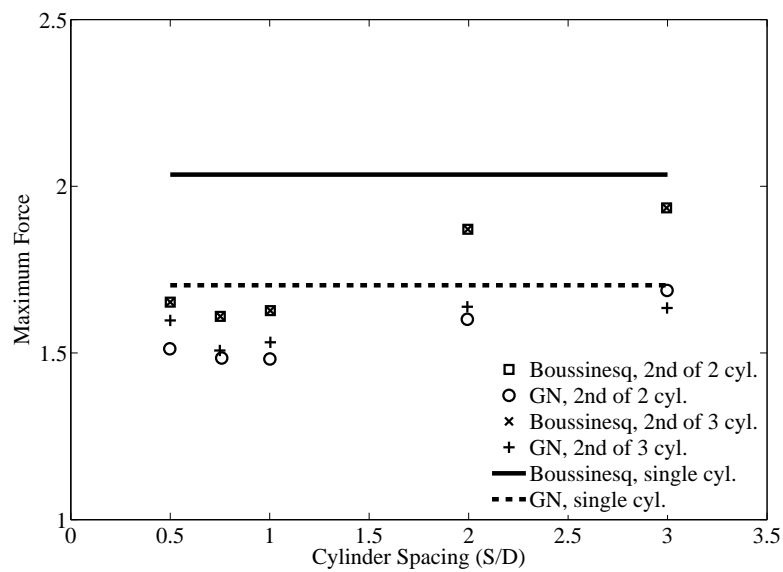


Fig. 19 Solitary wave maximum forces on the second cylinder, for one, two and three cylinders cases, versus cylinder spacing, $H = 0.5h$ and $D = 4.0h$

Accepted manuscript
edited by the journal

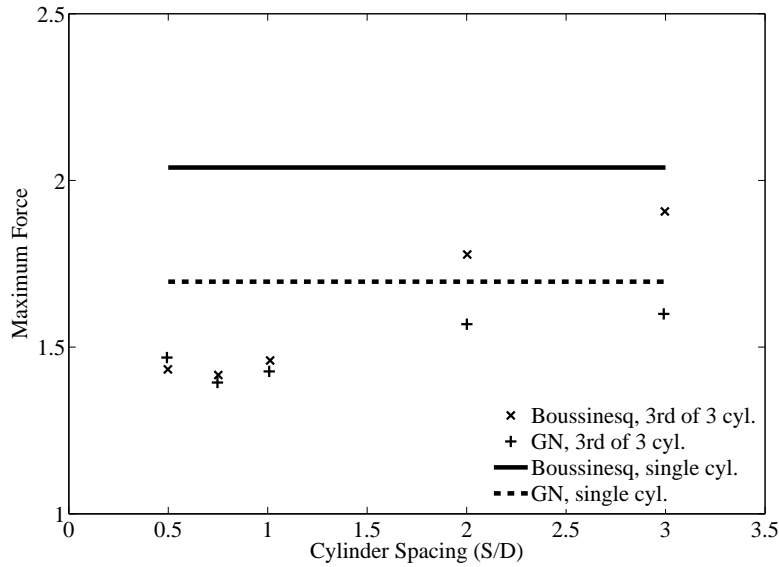


Fig. 20 Solitary wave maximum forces on the third cylinder, for one, two and three cylinders cases, versus cylinder spacing, $H = 0.5h$ and $D = 4.0h$

641 equations and the Boussinesq equations. The solution is formulated using a
 642 boundary-fitted curvilinear coordinate system that allows utilizing a finite-
 643 difference method in solving the problem. The wave-induced horizontal force
 644 and the overturning moment are obtained by integrating the pressure around
 645 the vertical cylinders. In the model developed based on the Green-Naghdi
 646 equations, the total pressure distribution around the vertical cylinders is ob-
 647 tained assuming a linear distribution of pressure over the water column. Ac-
 648 curacy and error associated with the numerical calculations can be assessed
 649 by monitoring the mass and moment throughout the computations.

650 Overall, close agreement is observed between the results of the Green-
 651 Naghdi equations and the Boussinesq equations with laboratory measurements
 652 and existing theoretical solutions. The performance of the Green-Naghdi equa-
 653 tions is found to be generally better than the Boussinesq equations. They pro-
 654 duce values for the forces and the moments that are in slightly closer agreement
 655 with both the experimental data and other predictions. The results of the GN
 656 equations and the Boussinesq equations are in closer agreement for smaller
 657 cylinder spacings.

658 It is found that the presence of the second and third cylinders on the wave
659 loads on all cylinders is significant in general. In a number of cases studied here,
660 the resultant loads on the first cylinder has increased due to the second and
661 third cylinders. Such effect is found to be a function of the distance between
662 the cylinders. This is in qualitative agreement with the results obtained for
663 wave interaction with an array of vertical cylinders in deep water. In all cases,
664 however, the first cylinder has provided shielding effect and the maximum
665 forces on the second and third cylinders are smaller than that on the first
666 cylinder. The shielding effect increases as the distance between the cylinders
667 decreases.

668 The Green-Naghdi equations cannot possess a moment equation, or an
669 equation for the pressure as a function of the water depth that can be used to
670 produce the moment. It is shown in this study that the Green-Naghdi equa-
671 tions can produce accurate predictions of moments when a linear distribution
672 of pressure with depth is assumed. The associated error to this assumption is
673 calculated and found to be negligible. The agreement between the moments
674 calculated through the Green-Naghdi equations and the generalized Boussi-
675 nesq equations is comparable to the agreement between the forces determined
676 by these methods, and the results are in good agreement with measurements
677 and analysis of laboratory experiments. Note that the assumption of linear
678 pressure variation over depth does not mean that the pressure is hydrostatic.

679 It is noted that it should be possible to solve the same physical problem by
680 use of higher levels of the GN equations that possess better nonlinearity and
681 dispersive characteristics, however, at a much greater computational effort.

Author accepted manuscript
Not copyedited by the journal

References

- 682 **References**
- 683 Barlas B (2012) Interactions of waves with an array of tandem placed bottom-
684 mounted cylinders. *J of Marine Science and Technology* 20(1):103–110
- 685 Burden RL, Faires JD (1985) *Numerical Analysis*, 3rd edn. Prindle, Weber &
686 Schmidt Publishers, Boston
- 687 Demirbilek Z, Webster WC (1992) Application of the Green-Naghdi theory of
688 fluid sheets to shallow water wave problems. Tech. Rep. CERC-92-11, US
689 Army Corps of Engineers, Vicksburg, Mississippi, 48 p.
- 690 Ertekin RC (1984) Soliton generation by moving disturbances in shallow wa-
691 ter: Theory, computation and experiment. PhD thesis, Ph.D. Dissertation,
692 University of California at Berkeley, May, v+352 pp.
- 693 Ertekin RC (1988) Nonlinear shallow water waves: The Green-Naghdi equa-
694 tions. In: *Proc. Pacific Congress on Marine Sci. and Techno., PACON '88,*
695 *Honolulu*, pp OST6/42–52
- 696 Ertekin RC, Webster WC, Wehausen JV (1986) Waves caused by a moving
697 disturbance in a shallow channel of finite width. *J Fluid Mechanics* 169:275–
698 292
- 699 Ertekin RC, Qian ZM, Wehausen JV (1990) Upstream Solitons and Wave
700 Resistance, World Scientific, New Jersey. Chapter in *Engineering Science,*
701 *Fluid Dynamics*, pp 29–43
- 702 Ertekin RC, Hayatdavoodi M, Kim JW (2014) On some solitary and cnoidal
703 wave diffraction solutions of the Green-Naghdi equations. *Applied Ocean*
704 *Research* 47:125–137, DOI: 10.1016/j.apor.2014.04.005
- 705 Ghadimi P, Bandari HP, Rostami AB (2012) Determination of the heave and
706 pitch motions of a floating cylinder by analytical solution of its diffraction
707 problem and examination of the effects of geometric parameters on its dy-
708 namics in regular waves. *International Journal of Applied Mathematical*
709 *Research* 1(4):611–633
- 710 Green AE, Naghdi PM (1976a) A derivation of equations for wave propagation
711 in water of variable depth. *Journal of Fluid Mechanics* 78:237–246
- 712 Green AE, Naghdi PM (1976b) Directed fluid sheets. *Proc of the Royal Society*
713 *of London Series A, Mathematical and Physical Sciences* 347(1651):447–473
- 714 Green AE, Naghdi PM (1977) Water waves in a nonhomogeneous incompress-
715 ible fluid. *J Applied Mechanics* 44(4):523–528
- 716 Green AE, Naghdi PM (1984) A direct theory of viscous flow in channels. *Arch*
717 *for Rat Mech and Analysis* 86(1):39–64

- 718 Han Y, Zhan JM, Su W, Li YS, Zhou Q (2015) Comparison of flow fields
719 induced by fixed and oscillatory vertical cylinders in regular waves using 3D
720 numerical model. *Ocean Engineering* 106:238–251, DOI 10.1016/j.oceaneng.
721 2015.06.050
- 722 Havelock TH (1940) The pressure of water waves upon a fixed obstacle on
723 water. *Proc Roy Soc London A* 175:409–421
- 724 Hayatdavoodi M, Ertekin RC (2015a) Nonlinear wave loads on a submerged
725 deck by the Green-Naghdi equations. *J of Offshore Mechanics and Arctic*
726 *Engineering* 137(1):011,102 (1–9), DOI: 10.1115/1.4028,997
- 727 Hayatdavoodi M, Ertekin RC (2015b) Wave forces on a submerged horizontal
728 plate. Part I: Theory and modelling. *J Fluids and Structures* 54(April):566–
729 579, DOI: 10.1016/j.jfluidstructs.2014.12.010
- 730 Hayatdavoodi M, Ertekin RC (2015c) Wave forces on a submerged horizon-
731 tal plate. Part II: Solitary and cnoidal waves. *J Fluids and Structures*
732 54(April):580–596, DOI: 10.1016/j.jfluidstructs.2014.12.009
- 733 Isaacson MQ (1978) Interference effects between large cylinders in waves. *Proc*
734 *10th Offshore Tech Conf, Houston, Vol. I(Paper No. OTC 3069):185–192*
- 735 Isaacson MQ (1983) Solitary wave diffraction around large cylinders. *J Wa-*
736 *terways, Port, Coastal and Ocean Eng* 109(1):121–127
- 737 Isaacson MQ, Cheung KF (1992) Time-domain second-order wave diffraction
738 in three dimensions. *J Waterways, Port, Coastal and Ocean Engineering*
739 118(5):496–517
- 740 Kagemoto H, Murai M, Saito M, Molin B, Malenica Š (2002) Experimental
741 and theoretical analysis of the wave decay along a long array of vertical
742 cylinders. *J of Fluid Mechanics* 456:113–135
- 743 Kamath A, Alagan Chella M, Bihs H, Arntsen ØA (2015) Evaluating wave
744 forces on groups of three and nine cylinders using a 3D numerical wave tank.
745 *Engineering Applications of Computational Fluid Mechanics* 9(1):343–354
- 746 Kudeih M, Cornett A, Nistor I (2010) An experimental study of wave and
747 current-induced forces on a compact linear array of vertical cylinders in
748 shallow water. *32nd Conference on Coastal Engineering, Shanghai, China*
749 1(32):10
- 750 Linton CM, Evans DV (1990) The interaction of waves with arrays of vertical
751 circular cylinders. *J Fluid Mechanics* 215:549–569
- 752 MacCamy RC, Fuchs RA (1954) Wave forces on a pile: a diffraction theory.
753 *Tech Memo 69, US Army Corps of Engineers*

- 754 Malenica S, Eatock Taylor R, Huang JB (1999) Second-order water wave
755 diffraction by an array of vertical cylinders. *Journal of Fluid Mechanics*
756 390:349–373, DOI 10.1017/S0022112099005273
- 757 McIver P, Evans D (1984) Approximation of wave forces on cylinder arrays.
758 *Applied Ocean Research* 6(2):101–107
- 759 Mei CC (1989) *The Applied Dynamics of Ocean Surface Waves*. World Scien-
760 tific, Singapore
- 761 Mo W (2010) Numerical investigation of solitary wave interaction with group
762 of cylinders. PhD thesis, Cornell University, xvi+169 p.
- 763 Mo W, Liu PLF (2009) Three dimensional numerical simulations for non-
764 breaking solitary wave interacting with a group of slender vertical cylinders.
765 *International Journal of Naval Architecture and Ocean Engineering* 1(1):20–
766 28
- 767 Neill DR (1996) The nonlinear interaction of waves with multiple, vertical, in-
768 line cylinders. Ph.D. Dissertation, Dept. of Ocean Engineering, University
769 of Hawaii
- 770 Neill DR, Ertekin RC (1997) Diffraction of solitary waves by a vertical cylinder:
771 Green-Naghdi and Boussinesq equations. *Proc 16th Int Conf on Offshore*
772 *Mechanics and Arctic Engineering, OMAE '97, ASME, Yokohama, Japan,*
773 I-B:63–71
- 774 Omer GC, Hall HH (1949) The scattering of a tsunami by a cylindrical island.
775 *Bulletin of the Seismological Society of America* 39(4):257–260
- 776 Qian ZM (1988) Numerical grid generation and nonlinear waves generated by
777 a ship in a shallow-water channel. M.S. Thesis, Dept of Ocean Engineering,
778 University of Hawaii, v+121 pp.
- 779 Qian ZM (1994) Calculations of three dimensional nonlinear ship waves and
780 ship resistance in a shallow water channel. Ph.D. Dissertation, Dept. of
781 Ocean Engineering, University of Hawaii
- 782 Rayleigh L (1876) On waves. *Phil Mag* I(5):257–279
- 783 Roddier D (1994) Diffraction and refraction of solitons around a false wall.
784 M.S. Thesis, Dept. of Ocean Engineering, University of Hawaii
- 785 Roddier D, Ertekin RC (1999) Diffraction and remodeling of solitons
786 around a false wall. *Chaos, Solitons and Fractals* 10(7):1221–1240
- 787 Shapiro R (1975) Linear filtering. *Mats Comput* 29:1094–1097
- 788 Shields JJ, Webster WC (1988) On direct methods in water-wave theory. *J*
789 *Fluid Mechanics* 197:171–199

- 790 Spring BH, Monkmeier PL (1974) Interaction of plane waves with vertical
791 cylinders. In: Proceedings of the 14th international conference on coastal
792 engineering, Copenhagen, Denmark, vol 107, pp 1828–1845
- 793 Teng M, Wu TY (1992) Nonlinear water waves in channels of arbitrary shape.
794 J Fluid Mechanics 242:211–233
- 795 Thompson JF, Thames FC, Mastin CW (1977) Boundary-fitted curvilinear
796 system for solutions of partial differential equations on fields containing any
797 number of arbitrary two dimensional bodies. Report No. CR2729, NASA
- 798 Wang KH, Jiang L (1994) Interactions of solitary waves with cylinder arrays.
799 In: Proc. 13th Int. Conf. on Offshore Mechanics and Arctic Engineering,
800 ASME, Houston, Texas, USA., vol I, pp 99–107
- 801 Wang KH, Wu TY, Yates GT (1992) Three-dimensional scattering of solitary
802 waves by vertical cylinder. J Waterway, Port, Coastal and Ocean Engineer-
803 ing, 118(5):551–566
- 804 Wu D, Wu TY (1982) Three-dimensional nonlinear long waves due to moving
805 surface pressure. In: Proc. 14th Symp. on Naval Hydrodynamics, Washing-
806 ton, D.C., National Academy Press, Washington, D.C., 1983, pp 103–125
- 807 Wu TY (1981) Long waves in ocean and coastal waters. J Engineering Me-
808 chanics Division 107(3):501–522
- 809 Yang C, Ertekin RC (1992) Numerical simulation of nonlinear wave diffrac-
810 tion by a vertical cylinder. J Offshore Mechanics and Arctic Engineering
811 114(1):36–44
- 812 Yates GT, Wang KH (1994) Solitary wave scattering by a vertical cylinder: Ex-
813 perimental study. Proc 4th Int Offshore and Polar Engineering Conference,
814 ISOPE '94, Osaka, Japan, III:118–124
- 815 Zhao BB, Duan WY, Ertekin RC (2014a) Application of higher-level GN the-
816 ory to some wave transformation problems. Coastal Engineering 83:177–189,
817 DOI:10.1016/j.coastaleng.2013.10.010
- 818 Zhao BB, Ertekin RC, Duan WY, Hayatdavoodi M (2014b) On the steady
819 solitary-wave solution of the Green–Naghdi equations of different levels.
820 Wave Motion 51(8):1382–1395, DOI:10.1016/j.wavemoti.2014.08.009
- 821 Zhao BB, Duan WY, Ertekin RC, Hayatdavoodi M (2015) High-level Green–
822 Naghdi wave models for nonlinear wave transformation in three dimen-
823 sions. Journal of Ocean Engineering and Marine Energy 1(2):121–132,
824 DOI:10.1007/s40,722–014–0009–8